Catal Lett (2015) 145:299–308
DOI 10.1007/s10562-014-1418-y

Charge Transport in Metal–Oxide Interfaces: Genesis and Detection of Hot Electron Flow and Its Role in Heterogeneous Catalysis

Sun Mi Kim · Hyosun Lee · Jeong Young Park

Received: 13 October 2014 / Accepted: 29 October 2014 / Published online: 8 November 2014

Abstract Most nanocatalysts are composed of highly dispersed transition metal nanoparticles on oxides. The interface between the metal nanoparticles and the oxides plays a crucial role in determining the catalytic performance of the nanocatalysts. Due to non-adiabatic electronic excitation, energetic electrons in metals can be generated during exothermic chemical processes. The energy barrier formed at the metal–oxide interfaces leads to the irreversible transport of energetic, or hot, electrons. The dopants and impurities present on the oxides can generate additional charge carriers or oxygen vacancies that affect the catalytic activity. The accumulation or depletion of hot electrons on the metal nanoparticles, in turn, can also influence the catalytic reactions. In this article, we outline recent studies of the role of metal oxide interfaces and characteristics of fast charge transfer between metals and oxides. The electronic configuration of metal–oxide nanocatalysts during catalytic reactions will be introduced and its influence on heterogeneous catalysis will be outlined.

Keywords Hot electron · Metal–oxide interface · Dopants · Oxygen vacancy · Heterogeneous catalysis

S. M. Kim · H. Lee · J. Y. Park (✉)
Center for Nanomaterials and Chemical Reactions, Institute for Basic Science, Daejeon 305-701, Republic of Korea
e-mail: jeongypark@kaist.ac.kr

S. M. Kim · H. Lee · J. Y. Park
Graduate School of EEWS, KAIST, Daejeon 305-701, Republic of Korea

1 Introduction

Industrial catalysts are mainly composed of metal particles in the 1–100 nm size regime dispersed in a high-surface-area support. They are produced by synthesizing the metal particles and support separately and then dispersing the metal clusters onto the support using various techniques (e.g., wet-impregnation, co-precipitation, or ion-exchange). The discontinuity between well-characterized model systems and industrially relevant catalysts represent the materials gap that has been a long-standing issue in heterogeneous catalysis [1–3].

One of the key issues in 'bridging materials gaps' is elucidating the role of metal–oxide interfaces in altering catalytic activity. The smart design of nanocatalysts can improve the catalytic activity of transition metals on reducible oxide supports. Figure 1a, b shows a scheme of the electronic configuration and the energy band diagram for metal–oxide interfaces under catalytic reactions. Electron excitation in exothermic catalytic reactions or the incidence of photons on metal surfaces results in the flow of high-energy electrons with an energy of 1–3 eV, assuming that most of the chemical or photon energy is converted to electron flow on a short (femtosecond) time scale before atomic vibration adiabatically dissipates the energy (picoseconds). The energetic electrons that are not in thermal equilibrium with the metal atoms are called "hot electrons". The Schottky barrier localized at the metal–oxide interface allows hot electrons to irreversibly transport through the interface.

There are a number of studies that indicate the significance of the metal–oxide interface. Earlier studies of Au/TiO_2 suggest that the perimeter area between the Au nanoparticles and TiO_2 is catalytically reactive under CO oxidation [4, 5]. This effect was also investigated by Boffa

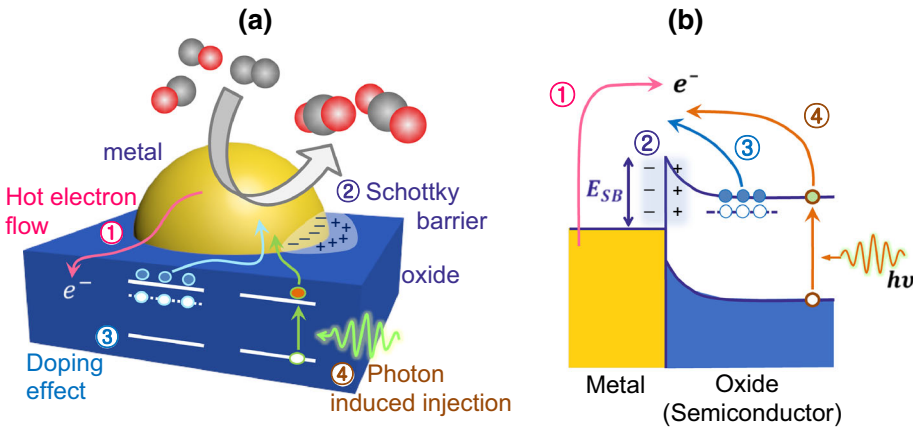

Fig. 1 **a** Electronic configuration and **b** energy band diagram of metal–oxide catalysts under chemical reactions illustrating (*1*) the flow of fast and energetic charge carriers, (*2*) formation of a Schottky barrier, (*3*) effect of dopants and oxygen vacancies, and (*4*) manipulation of hot carriers generated by photon absorption

et al. [6] using rhodium deposited on a large assortment of oxides. They observed a remarkable 14-fold increase in turnover rates for CO_2 hydrogenation, especially in the presence of three different oxides: TiO_x, NbO_x, and TaO_x. The activity was highest when the oxide–metal interface area was at a maximum, which occurred at ~0.5 monolayer of oxide coverage. On the other hand, several other oxides, including ZrO_x, VO_x, WO_x, and FeO_x, exhibit minor effects of coverage dependence. Interestingly, three oxides (i.e., TiO_x, NbO_x, and TaO_x) have bandgaps between 3.3 and 4.4 eV, which leads to the formation of a Schottky barrier between the oxides and the Rh film. These results indicate that the bandgap, or the presence of a Schottky barrier, plays a crucial role in determining the catalytic activity. Similar results on the effect of oxides on the catalytic activity of CO oxidation were also reported by Park et al. [7]. Doping or impurities in the oxides can result in excess charge carriers or oxygen vacancies on the oxides that lead to a change in catalytic activity [8, 9]. Additionally, charge accumulation or the depletion of hot electrons generated by photon absorption can be utilized to control catalytic activity, as illustrated in Fig. 1.

In this paper, we show the influence of metal–oxide interfaces on heterogeneous catalysis, focusing on the impact of electronic properties, including doping, bandgap, and Schottky barriers. We will outline the aspects of fast charge transfer between metal nanoparticles and oxides (semiconductors) that were uncovered using spectroscopic techniques with temporal resolution of femtoseconds. The correlation between the hot electron flows and catalytic activity under various exothermic reactions will be addressed.

2 Significance of Charge Transfer at Metal–Oxide Interfaces in Catalysis

When metal catalysts are mixed with semiconductor support materials, the composites show integrated and unprecedented properties that arise at the heterostructure interface. Enhancement of the catalytic activity on mixed catalysts was first investigated by Schwab [10, 11] and Solymosi [12]. These phenomena have been referred to as the "strong metal–support interaction" (SMSI), which was commonly used to describe the promoting and prohibiting effects of the support on the catalytic activity of the metal that cannot be explained as purely structural. Studies of the SMSI effect have increased in parallel with the advancement of diverse catalyst synthesis techniques and a variety of support materials that are improving the performance of supported catalysts. In particular, enormous efforts have been devoted to gaining a thorough understanding of the nature of the SMSI effect [13–16]. The general conclusion is that the interactions of the metal supports are influenced by three key properties: energetics of the metal particles (i.e., the properties reflecting the cohesive energy of a particle), geometric properties (e.g., those describing shape, size, crystal phase, order, strain, and structure), and electronic properties (e.g., those describing band structure, electron binding energies, and interactions of electrons with magnetic fields).

Among the various origins mentioned above, the predominant agreement is that the SMSI effect is ascribed to the alternation of the electronic structure of the metal by charge transfer to or from a support. Since metals normally have a smaller work function (Φ_m) than semiconductors, the energy bands (E_C and E_V) of the semiconductor are bent downwards when the two phases are in electric contact, as shown in Fig. 2a. Schwab's earlier results on mixed catalysts reveal a surprisingly superior action of the Ag/ZnO catalyst where silver (Ag) is combined with zinc oxide (ZnO). It is clear that for methanol oxidation, the mixed Ag/ZnO catalyst gives an extremely high yield of carbon dioxide (CO_2) and water vapor (H_2O) even at lower temperatures, in contrast with the individual catalysts (Ag and ZnO), as shown in Fig. 2b. This result can be explained by electron transfer from the metal into the semiconductor. Electrons have diffused from the metal into the

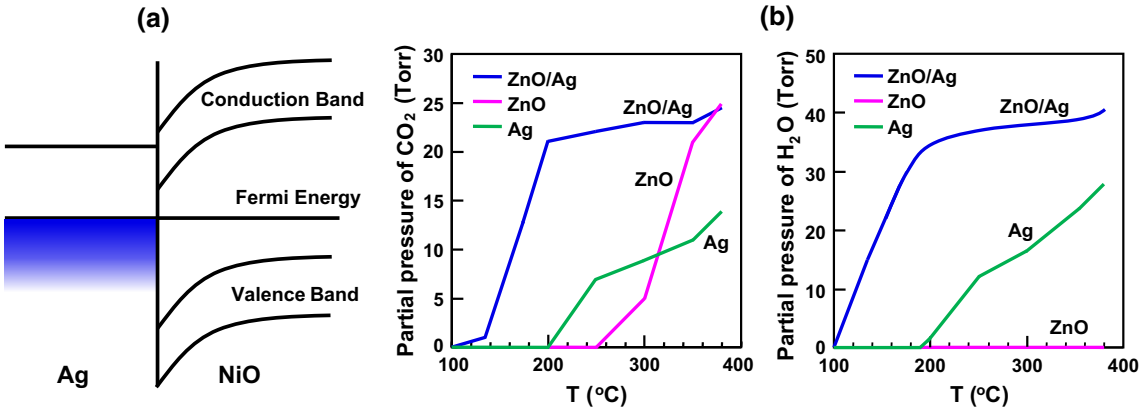

Fig. 2 **a** Band model of the inverse mixed metal–semiconductor catalyst, Ag/NiO, and **b** combined actions of the mixed metal–semiconductor Ag/ZnO catalysts: partial pressure of carbon dioxide (CO_2, *left*) and water vapor (H_2O, *right*) as a function of temperature. Reprinted from Ref. [10]. Copyright 2014, with permission from the American Chemical Society

semiconductor until their Fermi levels have equalized; the electron transfer thus influences the catalytic activity of the supported catalysts [17].

It is well known that the SMSI effect plays an important role in many catalytic reactions, although it is still unclear and under debate as to how the metal–support interface strongly influences surface chemistry and selectively amplifies specific reaction pathways. Figure 3 shows the catalytic activity and selectivity of platinum (Pt) nanoparticles supported on different metal oxides for hydrogenation of crotonaldehyde and the CO oxidation reaction, respectively [7, 18]. Regardless of the type of catalytic reaction, it is clear that the Pt nanoparticles show different catalytic activities according to the supported metal oxides. As shown in Fig. 3a, the support for the Pt nanoparticles has a substantial impact on the selectivity and activity of the catalyst for crotonaldehyde hydrogenation [18]. While the Pt/SiO_2 catalyst only produces the decarbonylation product propylene and the C=C bond hydrogenation product butyraldehyde, which are similar to those obtained on Pt (111) and (100) single crystals, the Pt/TiO_2 catalyst also produces 1-butanol and crotyl alcohol, the C=O hydrogenation products in addition to propylene and butyraldehyde. These results indicate that TiO_2 is deeply involved in the catalytic reactions occurring on the Pt nanoparticle surface. It was proposed, using sum frequency generation (SFG) vibration spectroscopy, that O-vacancy sites, the symbolic marker of the reduced TiO_2 support, are formed by the atomic contact of Pt and TiO_2, and it activates the production of alcohol products. Park et al. investigated the effect of the support in two-dimensional Pt nanoparticles on various metal oxide supports under CO oxidation [7]. As shown in Fig. 3b, the catalytic activity of Pt nanoparticles increases in the order of $CeO_2 > Nb_2O_5 > TiO_2 > SiO_2$; it is assumed that the redox capabilities of the oxide supports play an important

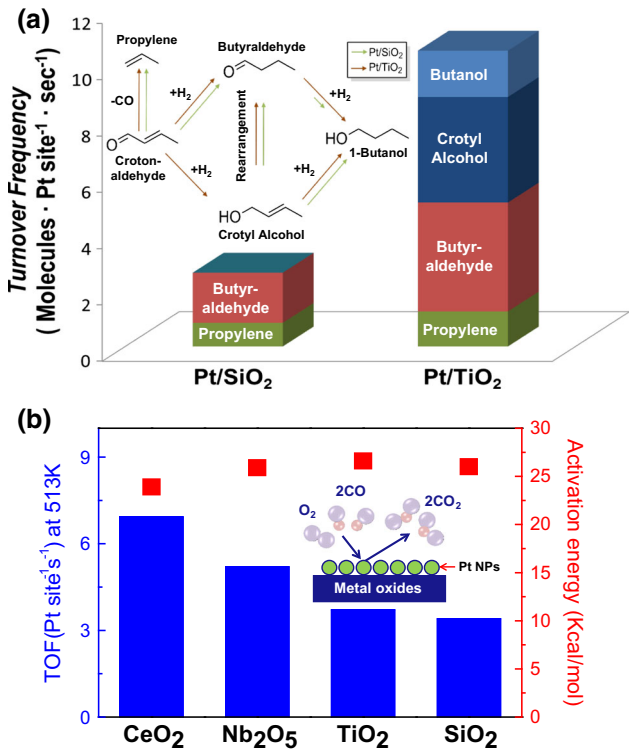

Fig. 3 **a** Turnover frequencies (TOFs) for the four observed products are reported for both the Pt/SiO_2 and Pt/TiO_2 catalysts. Similar rates of propylene production are observed for both catalysts. Butanol and crotyl alcohol production is only observed on the Pt/TiO_2 catalysts. (*Inset* Reaction scheme showing all the product pathways observed in the course of the reaction studies. Two sets of *arrows* represent the activity for each pathway for Pt/SiO_2 and Pt/TiO_2). **b** Summary of the TOFs at 513 K and activation energies for the CO oxidation reaction measured on colloidal 4.1 nm Pt nanoparticles. Reprinted from Ref. [7, 18]. Copyright 2014, with permission from Wiley–VCH Verlag GmbH & Co. KGaA, Weinheim [18] and Elsevier [7]

role in activating oxygen to react with the chemisorbed CO at the interface, controlling the activity of the Pt nanoparticles.

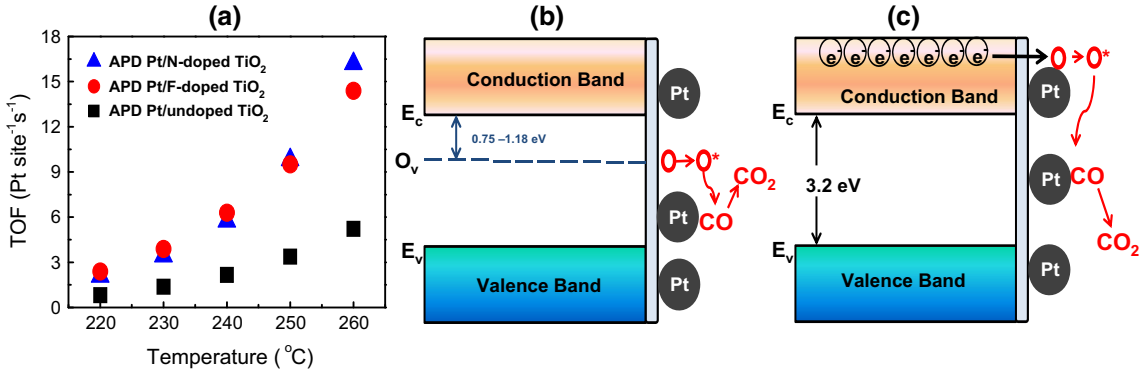

Fig. 4 Catalytic activity of CO oxidation results: **a** turnover frequencies (TOFs) of Pt nanoparticles on F-doped TiO_2, N-doped TiO_2, and undoped TiO_2. **b** Schematic diagram of the dissociation of O_2 by oxygen vacancies and the corresponding CO oxidation reaction on Pt/N-doped TiO_2 catalysts. **c** Schematic diagram of the proposed electronic activation mechanism of surface oxygen by charge transfer from the conduction band of TiO_2 to the adsorbed O on Pt/F-doped TiO_2 catalysts. Reprinted from Ref. [9]. Copyright 2014, with permission from Springer

Doping of the oxide is another way to tune the electronic states of the oxide supports and influences the chemical reaction process, resulting in changes in the catalytic activity and activation energy of catalysts [9]. Figure 4 shows the turnover rates of Pt nanoparticles on F-doped TiO_2, N-doped TiO_2, and undoped TiO_2 and the proposed mechanism to explain these CO oxidation results. As shown in Fig. 4a, the activities of the Pt nanoparticles supported on F- or N-doped TiO_2 are a factor of $\sim$2.5 higher than that of Pt nanoparticles on undoped TiO_2. These results indicate that the insertion of dopants changes the electronic states of the TiO_2 support, and that it drives the CO oxidation reaction. The proposed mechanisms for the enhancement of catalytic activity on N-doped and F-doped TiO_2 are shown in Fig. 4b, c, respectively. When nitrogen is doped into TiO_2, the oxygen vacancies are formed on the surface of the TiO_2 and it contributes to the dissociation of oxygen molecules and activation of the CO oxidation reaction (Fig. 4b). In the case of Pt/F-doped TiO_2, electron transfer from the conduction band of TiO_2 to the adsorbed oxygen forms an activated O^- intermediate that easily reacts with CO (Fig. 4c).

3 Detection of Fast Charge Transfer in the Temporal Regime on Metal–Oxide Interfaces

Gaining insight into the general dynamics of photoexcited charge carriers at metal–oxide interfaces is a fundamental step to study the role of metal–oxide interfaces and hot electron flows in heterogeneous catalysis. In this context, the spectroscopic investigation of various hybrid nanocomposites using ultrashort (picosecond and femtosecond) laser pulses in different wavelength regions (visible, infrared, UV, and X-ray) has been carried out [19–23]. Since ultrafast spectroscopy involves temporally short, therefore spectrally broad light pulses, this technique is useful to directly probe the dynamics of the system rather than the energy levels themselves. Mongin et al. investigated ultrafast charge separation in a model system of gold-tipped CdS nanorods with a matchstick architecture using the optical time-resolved pump–probe technique. Electron–hole pairs photoexcited in the semiconductor part of the nanohybrid catalyst underwent rapid charge separation where the electron transferred to the metal part on a sub-20 fs time scale [21]. Yu et al. utilized ultrafast spectroscopy to measure carrier dynamics in CdSe nanorods decorated with either Au or Pt metallic tips. Both hot and cold electrons transferring from the CdSe to the metal counterpart influence the rates of charge separation, which correlates with the photocatalytic H_2 evolution rate [23].

Figure 5 shows the dynamics of photoexcited carriers for CdSe, Pt–CdSe, and Pt–CdSe–Pt nanostructures using two-color pump–probe optical experiments [24]. In the pump–probe experiments, femtosecond pump pulses with a wavelength of 400 nm, obtained by frequency doubling fundamental pulses from a Ti:sapphire oscillator, are first used to excite the nanostructures; the probe pulses with energies near the band gap of the CdSe nanorods (625 nm for CdSe, 615 nm for Pt–CdSe and Pt–CdSe–Pt) were generated by doubling near-infrared femtosecond pulses from an optical parametric oscillator. The relative optical transmission change ($\Delta T/T$) of the probe pulse were measured as a function of time delay between the pump and probe pulses to monitor the carrier population at the band edge states of the CdSe nanorods, as shown in Fig. 5a, b. The temporal resolution, which was determined by the duration of the probe pulses, was around 250 fs. Nanostructures dispersed onto quartz substrates were measured with a pump intensity of 4 $\mu J/cm^2$ at the laser spot.

Figure 5c shows the time-resolved transmission change of the probe beam after photoexcitation by pump pulses at

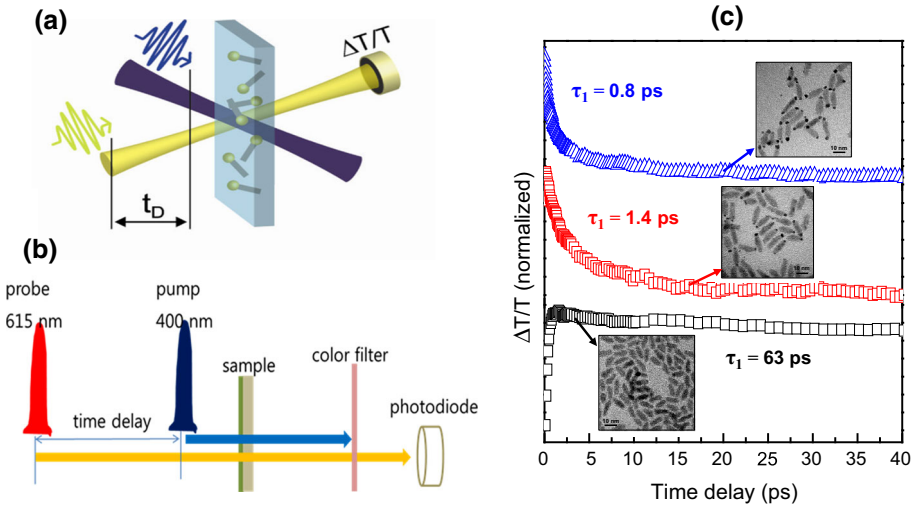

Fig. 5 Dynamics of photoexcited carriers for CdSe, Pt–CdSe, and Pt–CdSe–Pt nanostructures. **a** Principle and **b** schematic diagram of a time-resolved pump-probe optical experiment and **c** time-resolved transmission changes of the probe pulses near the band gap of the CdSe nanorods (625 nm for CdSe, 615 nm for Pt–CdSe and Pt–CdSe–Pt) are shown after photoexcitation by pump pulses at 400 nm (*black square* CdSe nanorod, *red square* Pt–CdSe nanorod, and *blue triangle* Pt–CdSe–Pt nanodumbbell). The bi-exponential fitting parameters of decay times and amplitudes are denoted for each data set. Reprinted from Ref. [21, 24]. Copyright 2014, with permission from the American Chemical Society

400 nm. Since the probe energy was adjusted to near the band gap of the CdSe nanorods, the observation of increased transmission can be explained by the photobleaching effect by carriers occupying the band edges of the CdSe nanorods. Due to ultrafast intraband relaxation of the photoexcited carriers to the band edges of the CdSe, the rise of the $\Delta T/T$ signal is almost instantaneous with a pump pulse for all of the structures. For CdSe nanorods, just 15 % of the signal peak decays within 40 ps. The extended scan data—up to 400 ps for CdSe nanorods—could be fitted to bi-exponential decays $A_1 \exp(-t/\tau_1) + A_2 \exp(-t/\tau_2)$ with time constants of $\tau_1 = 63$ ps ($A_1 = 0.163$) and $\tau_2 = 684$ ps ($A_2 = 0.80$ ps), which are possibly due to electron–hole recombination and carrier trapping at defects [25]. In a drastic contrast, the signals of the Pt–CdSe nanorods and Pt–CdSe–Pt nanodumbells decayed much faster. In less than 2 ps in the Pt–CdSe nanorods and 1 ps in the Pt–CdSe–Pt nanodumbells, the signal decayed to half of the signal peak. Decay constants of the bi-exponential fittings with correspondingly fast values are denoted in Fig. 5c. The pump-probe results demonstrate that additional paths are created in the hybrid nanostructures of CdSe and Pt where electrons can transfer from the CdSe semiconductor to the Pt metal.

Tachiya et al. have demonstrated the plasmon-induced charge transfer mechanism between an excited gold nanodot and a TiO_2 nanoparticle using ultrafast visible-pump/IR-probe femtosecond transient absorption spectroscopy [26–29]. Figure 6a shows the schematic diagram of photoinduced electron injection from a gold nanodot to a TiO_2 nanoparticle. When a ~550 nm laser light source is irradiated on the Au/TiO_2 nanoparticle system, electrons transfer from the plasmon band of the gold nanodots to the conduction band of the TiO_2 nanoparticle within 240 femtoseconds (the time resolution of the apparatus was obtained using a silicon plate), as shown in Fig. 6a. Here, the femtosecond IR-probe is used to identify the injected electrons in the TiO_2 conduction band from the gold nanodots, which are known to show strong intraband absorption in the IR region [30].

Figure 6b shows the transient absorption kinetics for Au/TiO_2 and N3/TiO_2 (N3 is a ruthenium complex dye) after correction for laser power as well as the corresponding absorption fraction for each sample. A remarkable point in Fig. 6b is the transient absorption signal of Au/TiO_2 that shows significant evidence of electrons being injected into the TiO_2 from the gold nanodot, while the Au/ZrO_2 doesn't show any transient absorption, meaning no electron transfer from the gold nanodots to the ZrO_2 at the probe wavelength (3,500 nm). Electrons injected into the TiO_2 nanoparticle are observed to decay through back electron transfer to the gold nanodots for times up to 1 ns. This back electron transfer process is dependent on the TiO_2 particle diameter, showing that it is slower when the TiO_2 particle size increases because the diffusion distances of free electrons within TiO_2 are farther before the electrons come back to the Au nanodot [27, 28]. N3/TiO_2 is a reference used to compare the electron injection yield because it is known to give an efficient charge separation yield of ~100 %, whereas the yield of Au/TiO_2 is estimated to be about 40 %, compared with N3/TiO_2.

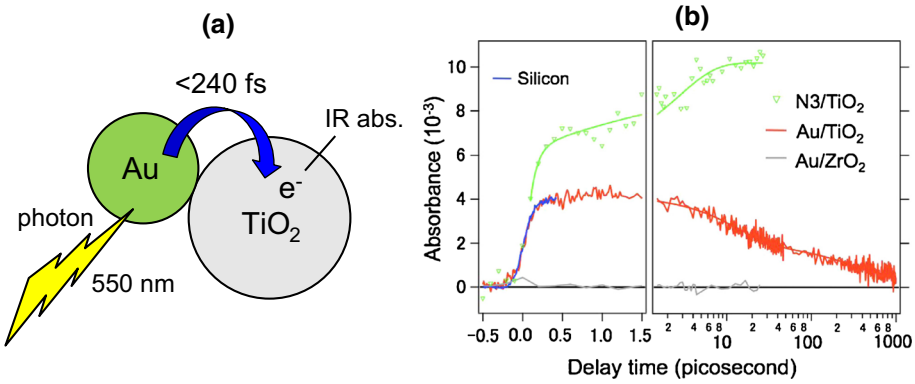

Fig. 6 **a** Schematic diagram of a gold nanodot attaching to a TiO_2 nanoparticle, also indicating the revealed electron injection process. **b** Transient absorption kinetics at 3,500 nm for nanocrystalline films (*green* $N3/TiO_2$, *red* Au/TiO_2, *gray* Au/ZrO_2). The *blue line* shows the response of the apparatus, obtained using a silicon plate. Reprinted from Ref. [29]. Copyright 2014, with permission from the American Chemical Society

4 Detection of Chemically Induced Hot Electrons Using Solid-State Devices

Over the last several decades, many scientists have made greater efforts to respond to the question regarding the role of hot electrons on surface chemical reactions, both theoretically and experimentally. As direct experimental evidence for electron-mediated energy transfer during chemical reactions, chemiluminescence and exoelectron emission have been reported in many studies since the 1970s [31–37]. In the dissociative chemisorption of halogen molecules on alkali metals, two electrons are typically transferred via two steps: the first electron is from the metal into the molecular affinity level accelerating dissociation, and the second electron can be either the emission of the excited electron into the vacuum (exoelectron emission) or the relaxation energy ($h\nu$) via photon generation (chemiluminescence) because of the unoccupied atomic affinity level on the metal surface. For detection of chemically induced exoelectrons or photons on the metal surface, the kinetic energy of the electron must have an energy greater than the work function of the metal, which is limited to the case of adsorption of a very electronegative atom or molecule onto a metal with a low work function in the range of 2–3 eV [38]. Therefore, it was hardly possible to observe the generation of hot electrons in common surface chemical reactions with lower exothermicity.

To observe the chemically induced electron excitations at transition metal surfaces constituting general heterogeneous catalysis, metal–semiconductor Schottky diodes (Ag/n-Si and Cu/n-Si) were suggested as a unique hot carrier detector by Nienhaus et al. in 1999 [39–41]. When the Ag or Cu film surfaces were exposed to thermal hydrogen or deuterium atoms, charge carriers excited at the surface were detected as chemicurrent in the diode. Figure 7a shows a schematic of the structure of the Schottky diode and the principle of current production. The thickness of the metal film on which the reaction occurs was determined considering the short elastic mean free path of electrons in metals (i.e., typically 10 nm). Excited electrons with sufficient energy (1–3 eV) can reach the metal–semiconductor interface ballistically without significant attenuation and move across the Schottky barrier, which is much lower than the metal work function, resulting in production of hot electron flows. The Schottky barrier height can be adjusted by changing the metal and interface properties. Furthermore, the direct detection of a hot hole injected from the metal film is also possible with a p-type Schottky diode and cannot be observed in emission experiments. Due to the several advantages of the devices, chemicurrent measurements have been carried out in various chemisorption reactions (e.g., H, O, Xe, NO, NO_2, C_2H_4, C_6H_6) on different metal surfaces in a series of studies [42], and confirmed that energy dissipation of the exothermic reaction on the metal surface is not effectively mediated by phonon excitation, but rather by electronic excitation.

Alternatively, tunnel devices, such as metal–insulator–metal (MIM) and metal–oxide–semiconductor (MOS), can also be used to detect electronic excitations created by exothermic reactions at the metal surface, as illustrated in Fig. 7b, c [38, 43, 44]. Since the tunneling mechanism allows excited electrons with somewhat lower energy to pass through the insulator layer, the transient chemicurrent was successfully measured when atomic and molecular gases (e.g., H, D, O, C_2H_4) were impinged on the Au top layer of $Au/TaO_x/Ta$(MIM) [45] and $Au/Al_2O_3/n$-Si (MOS) [43] tunnel junctions. Additionally, these tunnel devices allow for variation of the barrier by an external voltage due to displacement of the Fermi levels of the two materials with respect to each other, whereas Schottky diodes have a fixed barrier that cannot be adjusted by

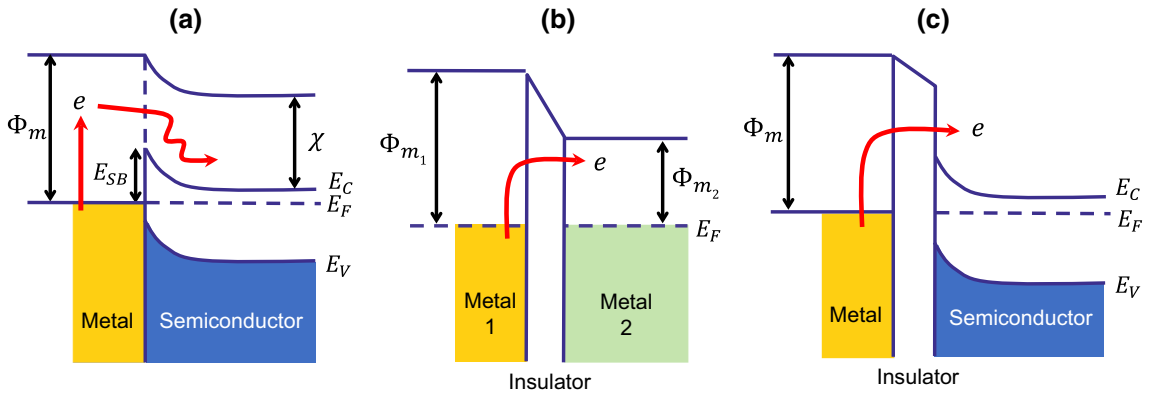

Fig. 7 Principle of chemicurrent detection with **a** an *n*-type Schottky diode, **b** a MIM tunnel device, and **c** a MOS device. Hot charge carriers excited during chemical reaction move ballistically from the metal surface to the interface. The top metal film thickness is typically in the 10 nm range. Reprinted from Ref. [43]. Copyright 2014, with permission from Elsevier

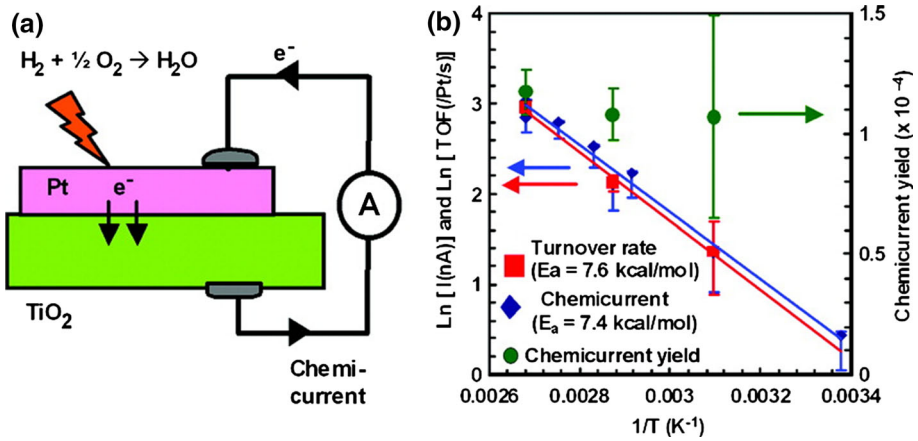

Fig. 8 **a** Schematic of hot electron generation on a Pt/TiO_2 Schottky diode during H_2 oxidation. The catalytic Pt film is very thin (~5 nm) to detect hot electron flows. **b** Arrhenius plots obtained from chemicurrent and turnover measurements on a Pt/TiO_2 diode with pressure of 6 Torr H_2 and 760 Torr O_2. The similar activation energies indicate that hot electron generation under hydrogen oxidation is proportional to the catalytic turnover rate. Reprinted from Ref. [55]. Copyright 2014, with permission from the American Chemical Society

applying an external electrical potential. If monitoring the dynamics of hot electrons under variable bias becomes feasible, it is expected to be utilized in spectroscopic study of hot electrons, which will provide profound insights into the distribution of energy during surface catalytic reactions.

5 Correlation Between Hot Electrons and Catalytic Activity in Metal–Oxide Nanostructures

Even though many experimental results have indicated that the metal–oxide interface plays a key role in determining catalytic activity, the origin of the strong metal–support interaction (SMSI) has not been clarified due to the lack of proper experimental measurement techniques [13, 46, 47]. The origin of enhanced catalytic activity at the metal–semiconductor interface has usually been attributed to either a geometric effect (i.e., charged metal surface at the interface) or electronic effect (i.e., charge transfer between the metal and the semiconductor) [13, 48]. Therefore, catalytic nanodiodes that are composed of a thin metal catalyst and an oxide have received great attention as an appropriate measurement technique to conclude the argument because it can simultaneously detect charge transfer through the metal–semiconductor interfaces while also taking turnover rate measurements.

Early experiments utilizing a metal–semiconductor Schottky diode to elucidate fundamental insights into the dynamics of chemical processes at metal surfaces were conducted at low-temperature and ultrahigh vacuum conditions [41]. Since 2005, however, Somorjai's group has extended this approach to high-temperature and -pressure systems that are identical to practical catalysis conditions [49, 50]. As a model system, oxidation of carbon monoxide

Table 1 Summary of activation energies on each type of diode in various chemical reactions

Type of diode	Reaction system	Partial pressure (Torr)	Activation energy (kcal/mol)		References
			Chemicurrent	Turnover rate	
Pt/TiO_2	CO oxidation	CO (40)/O_2 (100)	21.3 ± 0.7	22.4 ± 1.3	[49, 50]
Pt/GaN	CO oxidation	CO (40)/O_2 (100)	20.6 ± 1.1	21.3 ± 1.3	[50]
Pd/TiO_2	CO oxidation	CO (40)/O_2 (100)	20.4 ± 1.1	21.1 ± 0.9	[50]
Pt/TiO_2	H_2 oxidation	H_2 (6)/O_2 (760)	7.4 ± 0.3	7.6 ± 0.6	[52]
Rh/TiO_x	CO/NO reaction	CO (8)/NO (8)	25.4	26.1	[53]
Rh/GaN	CO/NO reaction	CO (8)/NO (8)	31.7	32.8	[53]

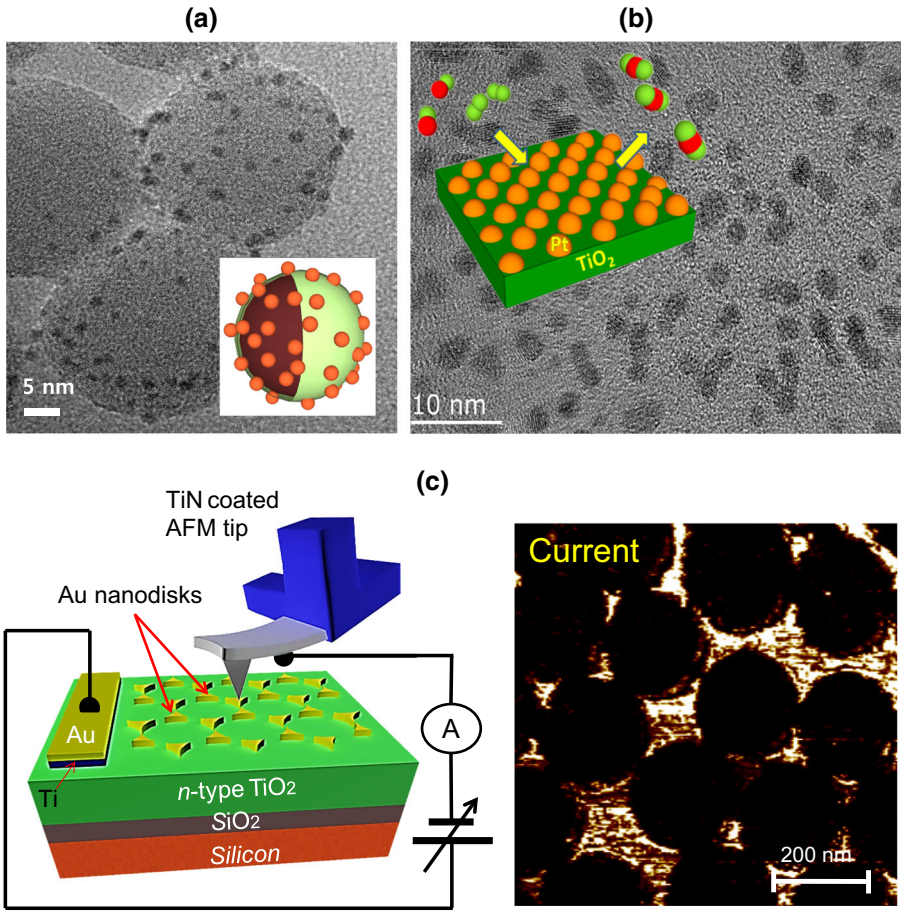

Fig. 9 **a** TEM image and scheme of a $Pt/SiO_2/TiO_2$ hybrid nanocatalyst [59]. **b** TEM images of Pt nanoparticles deposited with arc plasma deposition on a TiO_2 substrate [60]. **c** Scheme of AFM experiments on Au islands on a TiO_2 substrate (*left*) and conductance mapping (*right*) [61]. Reprinted from Ref. [43, 59–61]. Copyright 2014, with permission from the Royal Society of Chemistry [59], the American Chemical Society [60], and the American Institute of Physics [61]

on platinum was chosen where a total energy of 2.9 eV is released via several elementary reaction steps, including chemisorption of CO and O_2 molecules, dissociation to two O atoms, and formation of CO_2. They fabricated two types of catalytic nanodiode, Pt/TiO_2 and Pt/GaN, and carried out catalytic oxidation of CO under 100 Torr O_2 and 40 Torr CO at temperatures between 353 and 473 K [51]. Since hot electrons generated on the Pt surface during exothermic reactions have enough kinetic energy to overcome the Schottky barrier (1.2 eV), a steady-state current was observed, implying that the reaction occurred and that the product rapidly left the surface; whereas a transient current was generated from the chemisorption reaction because of the eventual surface saturation. This confirmed that the generation of hot electrons is proportional to the rate of CO oxidation on the Pt surface by comparing the chemicurrent with the accumulation of CO_2.

Later, Park et al. clearly verified a quantitative correlation between hot electrons and catalytic activity, showing that the activation energies of chemicurrent and turnover rate are very similar during exothermic reactions [52–55]. In every experiment, the effective chemicurrent was

obtained by excluding an additional electric current caused by a temperature gradient across the nanodiode, which is called the thermoelectric current. The activation energies were determined using the slope of the Arrhenius plot of chemicurrent or turnover rate as a function of temperature under exothermic reactions.

Figure 8a, b shows a scheme of the detection of ballistic hot electrons in the Pt/TiO_2 catalytic nanodiode and Arrhenius plots of both chemicurrent and turnover rate measurements under H_2 oxidation condition, respectively. The activation energy of hydrogen oxidation obtained from the chemicurrent through the Pt/TiO_2 nanodiode is 7.4 ± 0.3 kcal/mol, which is well-matched with that from the turnover rate (7.6 ± 0.6 kcal/mol) [55]. The similar activation energies imply that the chemicurrent originates from the catalytic reaction and that catalytic nanodiodes can replace turnover rate measurements (e.g., gas chromatography and mass spectroscopy). This phenomenon was not only confirmed by using other metal thin films, but also via various catalytic reactions [53, 55, 56]. Table 1 gives a summary of the activation energies obtained from chemicurrent and turnover rate, which were investigated under various reaction systems. Investigation of catalyzed reactions by catalytic nanodiodes, therefore, provides valuable insight into the role of electron excitation and flow in chemical reactivity of oxide-supported metal catalytic systems for various reactions.

6 Perspective and Concluding Remarks

The future direction of metal–oxide interface and hot electron research includes several topics, such as development of new model catalysts systems and surface characterization of metal–oxide interfaces, as shown in Fig. 9. Combined with the advancement of colloid chemistry and nanotechnology, new catalysts (e.g., nanoparticles with controlled size, shape, and composition; and multifunctional nanocatalysts, such as core–shell and yolk–shell) have been developed [57, 58]. Figure 9a shows hybrid metal–oxide nanocatalysts that can be model systems for investigating metal–oxide interfaces. Here, metal nanoparticles were deposited on functionalized SiO_2 and an ultrathin layer of TiO_2 was then selectively coated on the SiO_2 surface to prevent sintering and to provide high thermal stability, while maximizing the metal–oxide interface for higher catalytic activity [59]. The types of oxides and metal nanoparticles can be changed, thus allowing the catalytic properties of various combinations of metals and oxides to be tested within this framework.

Two-dimensional model catalysts are important because they can be well characterized using various surface techniques. Figure 9b shows two-dimensional arrays of metal nanoparticles, fabricated via arc plasma deposition that can be useful model systems to study the effect of the metal–oxide interface [60]. The nanoscale charge transport properties of metal–oxide systems can be studied by means of various surface techniques. For example, Lee et al. utilized conductive probe atomic force microscopy on Au nanoislands on TiO_2 to investigate the charge flows and the change in Schottky barrier height of nanosized islands, as shown in Fig. 9c [61]. Here, Au nanoislands were fabricated in self-assembled patterns on an n-type TiO_2 semiconductor film using the Langmuir–Blodgett process for the silica particles. Investigation of the physical, electronic, and chemical properties of metal–oxide interfaces and their influences on catalytic activity and selectivity is a key issue for "bridging the materials gap" and will be an active research area in heterogeneous catalysis.

In conclusion, we highlighted recent studies of the role of hot electron flows in surface chemistry and heterogeneous catalysis. We discussed the SMSI effects on various catalytic systems to address the role of the metal–oxide interface to determine the catalytic activity and selectivity of heterogeneous catalysis. Generation and detection of hot electron flows with several different schemes were shown. The strong correlation between hot electron generation and the turnover rates of catalyzed reactions were shown for several catalysts and reactions. We showed the spectroscopic study of fast charge transfer occurring at the interface between the metal and oxides with femtosecond time resolution. The developing research on new model catalysts with well-defined metal–oxide interfaces and microscopic techniques to probe nanoscale charge transport through metal–oxide interfaces was introduced.

Acknowledgments The work was supported by IBS-R004-G4.

References

1. Freund HJ, Kuhlenbeck H, Libuda J, Rupprechter G, Baumer M, Hamann H (2001) Top Catal 15:201
2. Somorjai GA, Park JY (2008) J Chem Phys 128:182504
3. Somorjai GA, York RL, Butcher D, Park JY (2007) Phys Chem Chem Phys 9:3500
4. Haruta M, Yamada N, Kobayashi T, Iijima S (1989) J Catal 115:301
5. Fujitani T, Nakamura I (2011) Angew Chem Int Edit 50:10144
6. Boffa A, Lin C, Bell AT, Somorjai GA (1994) J Catal 149:149
7. Park D, Kim SM, Kim SH, Yun JY, Park JY (2014) Appl Catal 480:25
8. Baker LR, Hervier A, Seo H, Kennedy G, Komvopoulos K, Somorjai GA (2011) J Phys Chem C 115:16006
9. Goddeti KC, Kim SM, Lee YK, Kim SH, Park JY (2014) Catal Lett 144:1411
10. Schwab GM, Koller K (1968) J Am Chem Soc 90:3078
11. Schwab GM (1969) Surf Sci 13:198
12. Solymosi F (1968) Catal Rev: Sci Eng 1:233

13. Hayek K, Fuchs M, Klotzer B, Reichl W, Rupprechter G (2000) Top Catal 13:55
14. Hu P, Huang Z, Amghouz Z, Makkee M, Xu F, Kapteijin F, Dikhtiarenko A, Chen Y, Gu X, Tang X (2014) Angew Chem Int Edit 53:3418
15. Tauster SJ, Fung SC, Baker RTK, Horsley JA (1981) Science 211:1121
16. Willinger MG, Zhang W, Bondarchuk O, Shaikhutdinov S, Freund HJ, Schlogl R (2014) Angew Chem Int Edit 53:5998
17. Schwab GM (1982) Crc Cr Rev Sol State 10:331
18. Kennedy G, Baker LR, Somorjai GA (2014) Angew Chem Int Edit 53:3405
19. Jailaubekov AE, Willard AP, Tritsch JR (2013) Nat Mater 12: 66 AE
20. Lei C, Bauer M, Read K, Tobey R, Liu Y, Popmintchev T, Murnane MM, Kapteyn HC (2002) Phys Rev B 66:245420
21. Mongin D, Shaviv E, Maioli P, Crut A, Banin U, Del Fatti N, Vallee F (2012) ACS Nano 6:7034
22. Tvrdy K, Frantsuzov PA, Kamat PV (2011) Proc Natl Acad Sci USA 108:29
23. Yu P, Wen XM, Lee YC, Lee WC, Kang CC, Tang J (2013) J Phys Chem Lett 4:3596
24. Kim SM, Lee SJ, Kim SH, Kwon S, Yee KJ, Song H, Somorjai GA, Park JY (2013) Nano Lett 13:1352
25. Klimov VI, McBranch DW, Leatherdale CA, Bawendi MG (1999) Phys Rev B 60:13740
26. Du L, Furube A, Hara K, Katoh R, Tachiya M (2009) Thin Solid Films 518:861
27. Du LC, Furube A, Hara K, Katoh R, Tachiya M (2013) J Photochem Photobiol C 15:21
28. Du LC, Furube A, Yamamoto K, Hara K, Katoh R, Tachiya M (2009) J Phys Chem C 113:6454
29. Furube A, Du L, Hara K, Katoh R, Tachiya M (2007) J Am Chem Soc 129:1485
30. Asbury JB, Hao E, Wang YQ, Ghosh HN, Lian TQ (2001) J Phys Chem B 105:4545
31. Greber T (1997) Surf Sci Rep 28:1
32. Hellberg L, Strömquist J, Kasemo B, Lundqvist BI (1995) Phys Rev Lett 74:4742
33. Kasemo B, Törnqvist E, Nørskov J, Lundqvist B (1979) Surf Sci 89:554
34. Kasemo B, Törnqvist E, Wallden L (1980) Mater Sci Eng 42:23
35. Kasemo B, Wallden L (1975) Surf Sci 53:393
36. Newns D, Makoshi K, Brako R, vaN WuNNik JNM (1983) Phys Scrip 1983:5
37. Ramsier R, Yates J Jr (1991) Surf Sci Rep 12:246
38. Nienhaus H, Gergen B, Weinberg W, McFarland E (2002) Surf Sci 514:172
39. Nienhaus H, Bergh H, Gergen B, Majumdar A, Weinberg W, McFarland E (1999) Phys Rev Lett 82:446
40. Nienhaus H, Bergh HS, Gergen B, Majumdar A, Weinberg WH, McFarland EW (1999) Appl Phys Lett 74:4046
41. Nienhaus H (2002) Surf Sci Rep 45:1
42. Gergen B, Nienhaus H, Weinberg WH, McFarland EW (2001) Science 294:2521
43. Liu X, Cuenya BR, McFarland E (2004) Sensors and Actuators B 99:556
44. Cuenya BR, Nienhaus H, McFarland EW (2004) Phys Rev B 70:115322
45. Mildner B, Hasselbrink E, Diesing D (2006) Chem Phys Lett 432:133
46. Penner S, Wang D, Podloucky R, Schlögl R, Hayek K (2004) Phys Chem Chem Phys 6:5244
47. Rupprechter G, Seeber G, Goller H, Hayek K (1999) J Catal 186:201
48. Haller GL, Resasco DE (1989) Adv Catal 36:173
49. Somorjai GA (2005) Catal Lett 101:1
50. Park JY, Renzas J, Contreras A, Somorjai GA (2007) Top Catal 46:217
51. Ji X, Zuppero A, Gidwani JM, Somorjai GA (2005) J Am Chem Soc 127:5792
52. Park JY, Somorjai GA (2006) ChemPhysChem 7:1409
53. Park JY, Renzas J, Hsu BB, Somorjai GA (2007) J Phys Chem C 111:15331
54. Park JY, Somorjai GA (2006) J Vac Sci Technol B 24:1967
55. Hervier A, Renzas JR, Park JY, Somorjai GA (2009) Nano Lett 9:3930
56. Renzas JR, Somorjai GA (2010) J Phys Chem C 114:17660
57. Joo SH, Park JY, Tsung CK, Yamada Y, Yang PD, Somorjai GA (2009) Nat Mater 8:126
58. Somorjai GA, Park JY (2008) Top Catal 49:126
59. Reddy AS, Kim S, Jeong HY, Jin S, Qadir K, Jung K, Jung CH, Yun JY, Cheon JY, Yang JM, Joo SH, Terasaki O, Park JY (2011) Chem Commun 47:8412
60. Qadir K, Kim SH, Kim SM, Ha H, Park JY (2012) J Phys Chem C 116:24054
61. Lee H, Lee YK, Van TN, Park JY (2013) Appl Phys Lett 103:173103